









Spatiotemporal patterns of intracellular Ca^{2+} signalling govern hypo-osmotic stress resilience in marine diatoms

Katherine E. Helliwell^{1,2} , Friedrich H. Kleiner^{1,3} , Hayley Hardstaff¹, Abdul Chrachri¹ , Trupti Gaikwad¹ , Deborah Salmon² , Nicholas Smirnoff² , Glen L. Wheeler¹  and Colin Brownlee^{1,3} 

¹The Laboratory, Marine Biological Association, Citadel Hill, Plymouth, PL1 2PB, UK; ²Biosciences, College of Life and Environmental Sciences, University of Exeter, Exeter, EX4 4QD, UK;

³School of Ocean and Earth Science, University of Southampton, Southampton, SO14 3ZH, UK

Authors for correspondence

Glen L. Wheeler

Email: glw@mba.ac.uk

Colin Brownlee

Email: cbr@mba.ac.uk

Received: 26 January 2020

Accepted: 11 December 2020

New Phytologist (2021)

doi: 10.1111/nph.17162

Key words: algae, Ca^{2+} signalling, diatoms, environmental sensing, osmotic stress, *Phaeodactylum*, R-GECO1, signalling.

Summary

- Diatoms are globally important phytoplankton that dominate coastal and polar-ice assemblages. These environments exhibit substantial changes in salinity over dynamic spatiotemporal regimes. Rapid sensory systems are vital to mitigate the harmful consequences of osmotic stress. Population-based analyses have suggested that Ca^{2+} signalling is involved in diatom osmotic sensing. However, mechanistic insight of the role of osmotic Ca^{2+} signalling is limited.
- Here, we show that *Phaeodactylum* Ca^{2+} elevations are essential for surviving hypo-osmotic shock. Moreover, employing novel single-cell imaging techniques we have characterised real-time Ca^{2+} signalling responses in single diatom cells to environmental osmotic perturbations.
- We observe that intracellular spatiotemporal patterns of osmotic-induced Ca^{2+} elevations encode vital information regarding the nature of the osmotic stimulus. Localised Ca^{2+} signals evoked by mild or gradual hypo-osmotic shocks are propagated globally from the apical cell tips, enabling fine-tuned cell volume regulation across the whole cell.
- Finally, we demonstrate that diatoms adopt Ca^{2+} -independent and dependent mechanisms for osmoregulation. We find that efflux of organic osmolytes occurs in a Ca^{2+} -independent manner, but this response is insufficient to mitigate cell damage during hypo-osmotic shock. By comparison, Ca^{2+} -dependent signalling is necessary to prevent cell bursting via precise coordination of K^+ transport, and therefore is likely to underpin survival in dynamic osmotic environments.

Introduction

Diatoms account for *c.* 40% of marine primary productivity (Falkowski *et al.*, 2004; Armbrust, 2009). This phylogenetically diverse group of microalgae are particularly prolific in coastal and estuarine regions, and constitute a major component of benthic intertidal biofilms (Underwood *et al.*, 1998). These environments are characterised by dynamic osmotic conditions (Kirst, 1990), with fluctuations in osmolarity ranging from gradual shifts to more sudden shocks (Lewin & Guillard, 1963). Intertidal, estuarine and rock pool habitats can encounter salinities ranging from 0‰ to 100‰ seawater or more, depending on river flow, rainfall and tidal action (Kirst, 1990). In addition, polar diatoms that inhabit sea-ice environments must adapt to living in the highly concentrated brine solution expelled during sea-ice formation, and then evade the damaging consequences of hypo-osmotic stress following ice melt (Kirst, 1990). Osmotic stress is therefore clearly an important environmental factor confronting natural diatom assemblages, living in a range of habitats.

Rapid shifts in osmolarity can lead to sudden changes in cell volume, which can have damaging consequences on cell

architecture and physiology (Paasche *et al.*, 1975; Kirst, 1990; Sarno *et al.*, 2007; Balzano *et al.*, 2011). Diatoms employ several mechanisms to mitigate the deleterious effects of osmotic stress. Cells exposed to elevated salinity (hyper-osmotic stress), accumulate inorganic ions (primarily K^+) and organic osmolytes including dimethyl sulfoniopropionate (DMSP), glycine betaine, and proline (Dickson & Kirst, 1987; Kirst, 1990), alongside cyclitols including cyclohexanetetrol (CHT) (Garza-Sánchez *et al.*, 2009). Species-specific differences in osmolyte usage are apparent. For instance, whereas CHT is the most abundant organic osmolyte in *Nitzschia ovalis* (Garza-Sánchez *et al.*, 2009), proline, glycine betaine and DMSP are the primary osmolytes in the model pennate diatom *Phaeodactylum tricornutum* (Schobert, 1980; Dickson & Kirst, 1987). Accumulation of proline and DMSP in hyper-osmotic environments, has also been observed in the polar species *Fragilariopsis cylindrus*, and is accompanied by enhanced synthesis capacity for these metabolites (Krell *et al.*, 2007). In contrast with hyper-osmotic shock, treatment with diluted seawater (i.e. hypo-osmotic stress) can lead to rapid dumping of osmolytes to avoid cell bursting. For instance, expulsion of

proline in response to reductions in salinity were observed within 1 h in *P. tricornutum* (Schobert, 1980).

Alongside metabolic adaptations to osmotic stress, morphological responses are known. Environmental osmotic conditions alter chain morphology and length in several *Skeletonema* species (Paasche *et al.*, 1975; Sarno *et al.*, 2007; Balzano *et al.*, 2011). Moreover *P. tricornutum*, which is pleomorphic, converts from planktonic fusiform or triradiate morphotypes, to benthic oval and round forms under hypo-osmotic conditions (De Martino *et al.*, 2011). This suggests that the distinct *P. tricornutum* morphotypes may confer different ecological advantages depending on the osmotic environment. Certainly, oval cells exhibit a number of unique features compared with the other *P. tricornutum* morphotypes, including a thicker, partially silicified cell wall, smaller vacuoles, lower surface-to-volume ratio, enhanced lipid content, and higher extracellular polysaccharide secretion (Francius *et al.*, 2008; De Martino *et al.*, 2011). It is possible that one or more of these features may be advantageous in a hypo-osmotic environment. However, the tolerance of different *P. tricornutum* morphotypes to hypo-osmotic shock, and the sensitivity and nature of their osmotic-signalling responses are so far unexplored. Furthermore, whilst some of the cellular and physiological strategies that diatoms employ to cope with osmotic stress are known, comparatively little is understood of how these osmo-acclimation responses are regulated.

Rapid signalling processes that regulate cell volume and mitigate the damaging consequences of osmotic stress are fundamentally important. In eukaryotes, calcium (Ca^{2+}) is a key player in signal transduction that regulates diverse physiological processes (Edel *et al.*, 2017). A role for Ca^{2+} in osmotic signalling has been identified in diverse eukaryotes (Takahashi *et al.*, 1997; Cessna *et al.*, 1998; Nakayama *et al.*, 2012; Bickerton *et al.*, 2016), including diatoms (Falcatore *et al.*, 2000). However, the nature of osmotic Ca^{2+} signalling varies considerably between taxa. For instance, hypo-osmotic stress, but not hyper-osmotic shifts, evokes intracellular Ca^{2+} elevations in *Chlamydomonas reinhardtii* (Bickerton *et al.*, 2016). By contrast, in higher plants (Archaeplastida) and the brown alga *Fucus* (stramenopiles), perception of both hyper- and hypo-osmotic adjustments entail Ca^{2+} -signalling-based processes (Taylor *et al.*, 1996; Takahashi *et al.*, 1997; Cessna *et al.*, 1998; Goddard *et al.*, 2000; Pauly *et al.*, 2001). In *Fucus* embryos, Ca^{2+} signals were vital for tolerating hypo-osmotic stress. In particular, stimulus-specific Ca^{2+} elevations that initiated in the vulnerable growing tip spread to the rest of the cell, and governed cell fate following hypo-osmotic shock (Goddard *et al.*, 2000). These studies highlight that Ca^{2+} signalling is essential for tolerating osmotic stress in many eukaryotes. However, fundamental differences in osmotic Ca^{2+} signals are clearly apparent (Taylor *et al.*, 1996; Takahashi *et al.*, 1997; Cessna *et al.*, 1998; Falcatore *et al.*, 2000; Goddard *et al.*, 2000; Pauly *et al.*, 2001; Bickerton *et al.*, 2016) and are likely to reflect the different adaptive mechanisms for coping with osmotic stress. Such fundamental differences highlight the need to examine the nature of this critical regulatory pathway in diverse eukaryotes.

In diatoms, work using the bioluminescent reporter aequorin revealed robust transient elevations of cytosolic Ca^{2+} in

populations of *P. tricornutum* in response to hypo-osmotic (but not hyper-osmotic) stress (Falcatore *et al.*, 2000). Removal of external Ca^{2+} abolished these hypo-osmotic-induced Ca^{2+} signals (Vardi *et al.*, 2006; Helliwell *et al.*, 2019). This work clearly points to an involvement of Ca^{2+} signalling in osmotic sensing in diatoms. However, mechanistic insight into the role of Ca^{2+} in the response to osmotic shock is lacking. In addition, an understanding of how diatom cells can distinguish distinct hypo-osmotic stimuli that differ in strength and/or rate of change, as could be encountered in nature, is limited. Furthermore, it is currently unknown how single-cell variability in hypo-osmotic-induced Ca^{2+} signals may impact cellular resilience to osmotic stress. Dose-dependent increases in Ca^{2+} signalling responses to increasing hypo-osmotic shocks have been observed in populations of *P. tricornutum* (Falcatore *et al.*, 2000). However, it is unclear whether this is a consequence of the increased amplitude of responses in individual cells or stimulation of a greater proportion of the population. An examination of single diatom cells is vital to address these important knowledge gaps.

We used single-cell imaging *P. tricornutum* cells expressing the fluorescent Ca^{2+} biosensor R-GECO1 (Zhao *et al.*, 2011; Helliwell *et al.*, 2019), to study diatom osmotic stress Ca^{2+} signalling. Using this approach it was possible to distinguish between multiple and repetitive signals at subcellular resolution. Our study uncovered distinct spatiotemporal patterns of osmotic-induced Ca^{2+} signals depending on the osmotic environment, and showed that such responses are essential for surviving severe hypo-osmotic shocks.

Materials and Methods

Cultivation of *P. tricornutum*

We obtained *Phaeodactylum tricornutum* strain CCAP1055/1 from the Culture Collection of Algae and Protozoa (SAMS Limited, Oban, UK). Cultures were maintained in artificial seawater (ASW) (450 mM NaCl, 30 mM MgCl_2 , 16 mM MgSO_4 , 8 mM KCl, 10 mM CaCl_2 , 2 mM NaHCO_3 , and 97 μM H_3BO_3) supplemented with f/2 nutrients (Guillard & Ryther, 1962; Guillard, 1975), with 100 μM $\text{Na}_2\text{SiO}_3 \cdot 5\text{H}_2\text{O}$, but not vitamins. For the Ca^{2+} -free ASW medium used for the experiments displayed in Figs 6–8, the same recipe for ASW was used, but 10 mM CaCl_2 was not included (and 200 μM EGTA was added). Cultures were illuminated with 50–80 $\mu\text{mol m}^{-2} \text{s}^{-1}$ light, on a 16 h : 8 h, light : dark cycle at 18°C. Oval cells were maintained on 1% ASW solid Bacto-agar plates (subbing every 4 d), and streaked onto glass-bottomed dishes containing 0.5 ml 1% ASW solid Bacto-agar and covered with 2 ml of 100% ASW.

Generation of fluorescent *P. tricornutum* lines expressing R-GECO1, R-GECO1 with GFP and GINKO1

The transgenic *P. tricornutum* lines described in this study (expressing R-GECO1, R-GECO1 with GFP and GINKO1) were generated as outlined in Supporting Information Methods S1.

Epifluorescence imaging in *P. tricornutum*

P. tricornutum cells grown in liquid culture for 72 h were placed in a 35 mm glass-bottomed dish (*In Vitro* Scientific, Sunnyvale, CA, USA) coated with 0.01% poly-L-lysine (Sigma-Aldrich, St Louis, MO, USA). Cells that adhered to the bottom of the dish were subsequently imaged at 20°C. Ca^{2+} imaging of R-GECO1 (PtR1) cells was performed using a Nikon Eclipse Ti microscope with a $\times 40$ magnification, 1.30 NA oil immersion objective and detection with a Photometrics Evolve EM-CCD camera (Photometrics, Tucson, AZ, USA). During imaging, cells were continuously perfused with ASW (3 ml min⁻¹), and hypo-osmotic shock treatments were delivered by switching the perfusion from ASW to the diluted ASW treatment. Excitation of PtR1 cells was performed using a pE2 excitation system (CooLED, Andover, UK) with 530–555 nm excitation and 575–630 nm emission filters. Images were captured using NIS-ELEMENTS v.3.1 software (Nikon, Japan) with a 300 ms camera exposure (frame rate of 3.33 frames s⁻¹). Epifluorescence imaging of GINKO1 (PtGINKO1) cells was performed using the same imaging set up, but with 475–490 nm excitation and 495–550 nm emission filters, and a 500 ms camera exposure (frame rate of two frames per second).

Dual imaging of the PtR1-GFP line (for simultaneous imaging of R-GECO1 and GFP fluorescence) was carried out using a DMi8 Inverted Microscope with a Photometric-Prime95B camera equipped with a Gemini W-View beamsplitter (emission filters 505–535 nm and 565–595 nm). Excitation of GFP and R-GECO1 fluorescence was at 470 nm and 550 nm, respectively.

For the confocal imaging of PtR1 cells (as displayed in Fig. 1a) a LEICA SP8 inverted confocal microscope was used, with a $\times 63$ 1.40 oil immersion objective. Excitation at 561 nm and emission at 572–600 nm was used for R-GECO1 fluorescence. For chlorophyll fluorescence the excitation wavelength was 633 nm and emission was detected at 657–675 nm.

Image processing and analysis

PtR1 and PtGINKO1 images were processed using NIS-ELEMENTS v.3.1 software. The mean fluorescence amplitude within a region of interest (ROI) over time was measured for each cell. For the majority of the image analyses, ROIs were drawn around the whole cell, unless a subcellular region was specified, for example for characterisation of $[\text{Ca}^{2+}]_{\text{cyt}}$ elevations in the tips of the cell or for the nuclear Ca^{2+} imaging (where ROIs were drawn in the nuclear region of the cell adjacent to the chloroplast). Change in fluorescence amplitude of R-GECO1 was calculated by normalising each trace by the initial value (F/F_0). As background fluorescence for PtR1 and PtGINKO1 was minimal, we did not carry out a background subtraction. However, a background subtraction was required for the PtR1-GFP dual imaging set up. $[\text{Ca}^{2+}]_{\text{cyt}}$ elevations were defined as any increase in F/F_0 fluorescence above a threshold value of 1.15. We calculated that an $F/F_0 \geq 1.15$ required a minimum signal-to-noise ratio (SNR) of 8, with SNR defined as signal intensity/SD of the background (i.e. noise). To visualise the Ca^{2+} elevations within cells, pseudo-coloured images representing the change in fluorescence (F/F_0)

were generated using IMAGEJ software (Schneider *et al.*, 2012). For this an ' F_0 ' image was first generated by averaging the first five frames of the stack. Each individual image was then divided by the F_0 image to generate a series of ' F/F_0 ' images.

Hypo-osmotic shock Ca^{2+} -imaging experiments

P. tricornutum cells grown in liquid culture for 72 h were imaged by epifluorescence microscopy. Rapid shifts in hypo-osmotic conditions were delivered by switching the perfusion from ASW (without nutrients) to ASW diluted with distilled water. Cells exposed to hypo-osmotic shock in the absence of Ca^{2+} were preperfused with at least 30 ml Ca^{2+} -free medium (+200 μM EGTA) (corresponding to *c.* 5 min). Gradual shifts in osmolarity were generated using a gradient mixer consisting of a main chamber (containing ASW) and a feeding chamber (with MilliQ water). A magnetic stirrer was used to mix the main chamber as the valve was opened (with a flow speed of 16 ml min⁻¹).

Imaging of *P. tricornutum* cells stained with vacuolar membrane dye MDY-64

Vacuolar membrane dye MDY-64 (Invitrogen) was used to stain *P. tricornutum* tonoplast membranes, as previously reported (Huang *et al.*, 2016). We added 1 μl of a 0.1 mM stock (diluted in DMSO) to 500 μl of wild-type (WT) *P. tricornutum* cells (final concentration of 0.2 μM). Cells were bathed in a glass-bottomed dish for 2 min before hypo-osmotic shock treatment. MDY-64 was excited with a 470 nm LED (CooLED), with a 500–550 nm emission filter. As *P. tricornutum* cells usually possess two large vacuoles either side of the central cytoplasmic region containing the nucleus and chloroplast, we defined 'tonoplast rupture' as the clear loss of both of these large vacuole structures by the end of the 60 s hypo-osmotic shock treatment.

Quantification of the Ca^{2+} dependency of organic osmolyte and K^+ efflux in *P. tricornutum*

Sample preparation and quantification methods for organic osmolyte measurements, and K^+ efflux experiments are given in Methods S2.

Results

Phenotypic plasticity in Ca^{2+} -signalling responses is apparent between cells exposed to repeated hypo-osmotic shocks

We have previously generated a transgenic line of *P. tricornutum* (PtR1) expressing the genetically encoded fluorescent Ca^{2+} indicator R-GECO1 in the cytosol (Zhao *et al.*, 2011; Helliwell *et al.*, 2019) (Fig. 1a). To examine hypo-osmotic Ca^{2+} signalling responses within individual PtR1 cells, we employed live-cell epifluorescence imaging, coupled with a controlled perfusion system. Treatment of cells with 60% artificial seawater (ASW) diluted with ddH₂O led to rapid single elevations in cytosolic

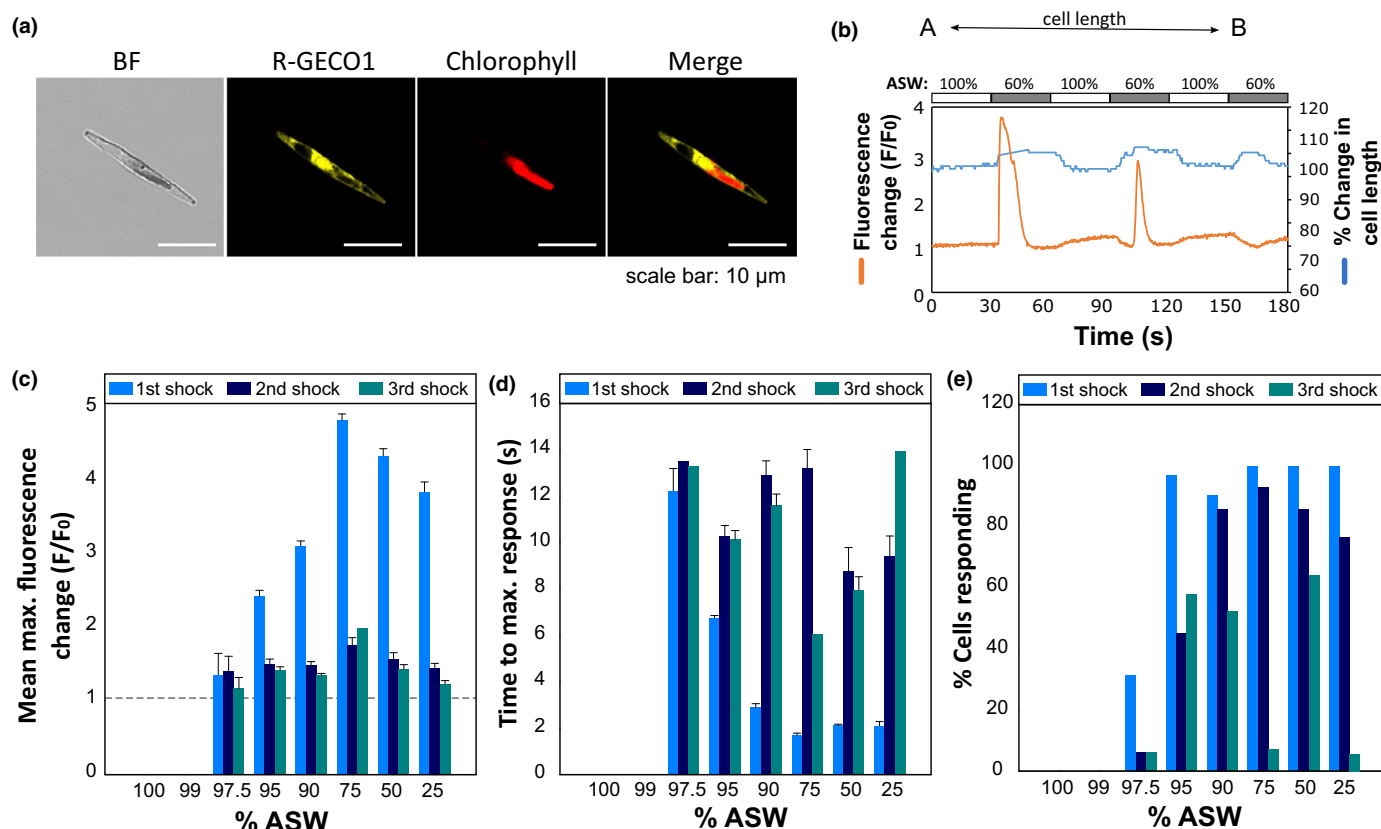


Fig. 1 Phenotypic plasticity in Ca^{2+} -signalling responses is apparent between cells exposed to repeated hypo-osmotic shock. (a) Confocal laser microscopy image of a *Phaeodactylum tricornutum* PtR1 cell demonstrating R-GECO1 fluorescence in the cytosol (yellow), along with chlorophyll autofluorescence (red). A bright field (BF) image is also displayed. Bars, 10 μm . (b) Representative trace of fluorescence changes (amplitude) over time of a PtR1 cell exposed to three successive 30 s hypo-osmotic shocks from 100% to 60% artificial seawater (ASW). The % change in cell length is also shown, measuring the length between the apical cell tips (schematic, above graph). Hypo-osmotic shocks were elicited at 30, 90 and 150 s (grey), and between each shock cells were returned to standard 100% ASW medium for 30 s before the next treatment (white). (c) Mean maximal fluorescence (F/F_0) of cells exposed to three successive hypo-osmotic shocks (data from the 1st shock, 2nd shock and 3rd shock are colour coded and labelled in the key) with ASW at a range of dilutions. The experiment was repeated three times with a different sample of cells, and a minimum total of $n = 14$ cells was examined per treatment. Only cells that exhibited a $[\text{Ca}^{2+}]_{\text{cyt}}$ elevation (above F/F_0 threshold of 1.15) were included (mean \pm SEM). Baseline fluorescence (i.e. $F/F_0 = 1$) is indicated with a dashed grey line. (d) Mean time to maximum response (s) following successive hypo-osmotic shocks with ASW at a range of dilutions as described in (c). Data from the 1st shock, 2nd shock and 3rd shock are colour coded and labelled in the key (error bars: SEM, $n \geq 14$). (e) Percentage of cells exhibiting a $[\text{Ca}^{2+}]_{\text{cyt}}$ elevation > 1.15 (relative to the fluorescence just before the shock) to successive hypo-osmotic shocks with ASW at a range of dilutions as described in (c).

Ca^{2+} that attenuated upon successive exposures (Fig. 1b). For the third exposure, F/F_0 values drifted below 1, most likely due to intracellular rearrangement resulting from repetitive exposures. Elevations in intracellular Ca^{2+} in response to hypo-osmotic shock were closely coupled with increases in cell length (Fig. 1b). The timing of the Ca^{2+} elevations in response to the first hypo-osmotic shock apparently occurred simultaneously with increases in cell length. However, upon exposure to the second shock, changes in cell length preceded the $[\text{Ca}^{2+}]_{\text{cyt}}$ elevation. These data demonstrate that hypo-osmotic shock causes cell swelling followed by transient elevations in cytosolic Ca^{2+} . To check that alterations in cell size were not responsible for the observed changes in R-GECO1 fluorescence, we generated a *P. tricornutum* clone encoding both R-GECO1 and GFP (PtR1-GFP) (Methods S1), and exposed cells to a 60% ASW hypo-osmotic shock treatment (Fig. S1). These experiments revealed that

GFP fluorescence did not change substantially from baseline fluorescence upon exposure to hypo-osmotic shock, and therefore indicated that increases in R-GECO1 fluorescence were due to changes in cytosolic Ca^{2+} concentrations, rather than to artefacts caused by more general alterations in cell volume.

Previous work demonstrated that the amplitude of Ca^{2+} -signalling responses in populations of *P. tricornutum*, increased with stronger hypo-osmotic shocks (Falcatore *et al.*, 2000). We tested whether this effect was due to an increased proportion of responding cells and/or a greater amplitude in $[\text{Ca}^{2+}]_{\text{cyt}}$ elevations. We exposed cells to hypo-osmotic shocks ranging from 99% ASW to 25% ASW (Fig. S2). The intensity of the responses varied according to stimulus strength (Fig. 1c) (Falcatore *et al.*, 2000), although the maximal fluorescence (F/F_0) plateaued with the strongest hypo-osmotic shock treatments (i.e. 50% and 25% ASW). The time from stimulus to response also tended to

decrease with stronger shock strength, and increased with successive exposures (Fig. 1d). Notably, examination of individual cell responses revealed single-cell variability. For instance, only 31.3% of cells responded to first exposure to 97.5% ASW (above F/F_0 threshold of 1.15) (Fig. 1e). Moreover, pre-exposure to osmotic shock influenced the propensity of cells to respond to successive shocks. For instance, whereas 100% of cells responded to first exposure to 50% ASW, 85.7% responded the second time, and 64.3% to the third. Similarly, upon second exposure to 95% ASW the mean maximal F/F_0 (including all cells within the population and including those that did not respond) was 1.25 ± 0.05 ($n=31$, SEM). However, within this population only 45% of cells gave a response with an average F/F_0 of 1.49 ($n=14$). Our data illustrated that, in addition to differences in signal amplitude, the proportion of responding cells correlated with stimulus strength, suggesting that a threshold needed to be reached for cells to respond. Therefore, bulk population averages did not convey the intricate dynamics and significant single-cell variability within diatom populations well.

Hypo-osmotic shock induces stimulus-strength dependent subcellular patterns of $[Ca^{2+}]_{\text{cyt}}$ and $[Ca^{2+}]_{\text{nuc}}$

We observed that cell swelling occurred as a consequence of hypo-osmotic shock, which precedes cytosolic Ca^{2+} elevations. Moreover, the nature of the osmotic stimulus influenced the amplitude, the proportion of cells responding and temporal properties of $[Ca^{2+}]_{\text{cyt}}$ elevations in *P. tricornutum*. This suggested that Ca^{2+} signalling responses convey important information regarding strength of the stimulus. In embryos of the multicellular brown alga *Fucus*, Ca^{2+} waves induced by hypo-osmotic shock propagated from the sensitive apex to the rest of the cell and these spatial properties had important outcomes on cell division (Goddard *et al.*, 2000). We therefore determined whether Ca^{2+} elevations in diatoms also displayed distinct spatial patterning, based on stimulus strength and reflecting differential sensitivity within regions of the cell. Examination of *P. tricornutum* cells exposed to different levels of hypo-osmotic shock revealed that many of the $[Ca^{2+}]_{\text{cyt}}$ elevations caused by mild hypo-osmotic shocks (95% ASW) initiated in the apical tip before spreading to the rest of the cell (13 out of 20 cells examined exhibited propagating Ca^{2+} elevations, the remaining 7 cells exhibited Ca^{2+} elevations that arose simultaneously across the whole cell) (Fig. 2a,b; Video S1). The average speed for the Ca^{2+} wave propagation was $37.1 \mu\text{m s}^{-1} \pm 6.0$ ($n=13$, SEM; including only cells initiating in one of the cell tips). By contrast, 50% ASW caused a rapid and transient Ca^{2+} elevation that arose simultaneously along the length of the cell (8/8 cells) (Fig. 2a,b; Video S2). Maximal fluorescence (F/F_0), was greatest at the cell tips compared with the centre of the cell, although this effect was most pronounced following the 95% ASW treatment (Fig. 2c), compared with the stronger 75% ASW shock (Fig. 2d). This was particularly noticeable with repeat shocks, for which Ca^{2+} elevations were almost undetectable in the centre of the cell, compared with the cell tips upon exposure to a second hypo-osmotic shock (Fig. S3). The mean time between the Ca^{2+} elevations in the tip regions (measured by comparing the

time between maximal fluorescence in each tip) (Fig. 2c,d), decreased with stronger treatments (Fig. 2e). In all hypo-osmotic treatments the first shock caused Ca^{2+} elevations that were apparent in all cell regions (detected in both tips) (Fig. 2f). However, the propensity of the signal to remain localised to just one tip (or to be absent entirely) increased in successive shocks, particularly with more mild shocks. Together these data pointed to an important role for the apical tip regions in sensing osmotic stress, whereby weaker stimuli resulted in a localised Ca^{2+} elevation in the tip(s) that can propagate information to the rest of the cell. By contrast, more severe hypo-osmotic shocks resulted in a response that occurred simultaneously across the whole cell. Therefore, stimulus-specific temporal and spatial Ca^{2+} -signalling patterns, encode important information on the nature of the environmental change experienced by the cell.

Dynamic changes in $[Ca^{2+}]_{\text{cyt}}$ are clearly integral to diatom responses to hypo-osmotic conditions. However, accumulating evidence indicates that distinct organellar compartments such as the nucleus can influence cellular Ca^{2+} signalling pathways. Nuclear- Ca^{2+} signals are reported to be particularly important in governing responses to osmotic stress (Goddard *et al.*, 2000; Pauly *et al.*, 2001; Huang *et al.*, 2017). *Fucus* rhizoid cells show distinct $[Ca^{2+}]_{\text{nuc}}$ elevations in response to hypo-osmotic stress that were dependent on stimulus strength (Goddard *et al.*, 2000). Such nuclear Ca^{2+} transients are likely to directly link to transcriptional regulation, and thus could control distinct physiological outcomes (Bootman *et al.*, 2009). To investigate how $[Ca^{2+}]_{\text{cyt}}$ elevations translate to changes in Ca^{2+} levels in the nucleus, we generated a transgenic *P. tricornutum* line expressing R-GECO1 (fused to nuclear-localised Histone H4) in the nucleus (strain PtR1-N) (Rosenwasser *et al.*, 2014). The specific growth rate of PtR1-N did not differ from the PtR1 line ($0.15 \text{ h}^{-1} \pm 0.005$ (SEM) and $0.14 \text{ h}^{-1} \pm 0.001$, respectively; Student's *t*-test, $P=0.102$). Similar to the cytosol, robust Ca^{2+} elevations that attenuated upon successive exposures were observed in the nucleus of fusiform cells following sequential treatments with 50% ASW (Fig. 3a,b). However, unlike in the cytosol in which 96.8% of cells responded even to subtle (95% ASW) shocks upon first exposure (Fig. 1e), we detected a nuclear response in only 21.4% of cells (Fig. 3c). Thus the lower amplitude propagating $[Ca^{2+}]_{\text{cyt}}$ elevations generated by exposure to 95% ASW did not give rise to distinct $[Ca^{2+}]_{\text{nuc}}$ elevations (Fig. 2a). A simple explanation for this is that the propagating $[Ca^{2+}]_{\text{cyt}}$ elevations induced by 95% ASW resulted in a much smaller increase in $[Ca^{2+}]_{\text{cyt}}$ in the central perinuclear region of the cell (Fig. 2c), compared with the global $[Ca^{2+}]_{\text{cyt}}$ elevations induced by 75% ASW (Fig. 2d). It therefore seems likely that this contributes to the lower incidence of $[Ca^{2+}]_{\text{nuc}}$ elevations at 95% ASW. However, similar to $[Ca^{2+}]_{\text{cyt}}$ elevations, the time from stimulus to response for $[Ca^{2+}]_{\text{nuc}}$ elevations tended to increase with successive exposures, albeit in general the time to maximum response was longer for nuclear than for cytosolic elevations (Figs 1d, 3d). It should be noted that for the PtR1 line, R-GECO1 was not fused to a nuclear export signal (Keinath *et al.*, 2015), although the relatively small size of the nucleus in *P. tricornutum* meant that the R-GECO1 signal reflected predominantly the perinuclear cytosol in that region. Our results suggested a stimulus-

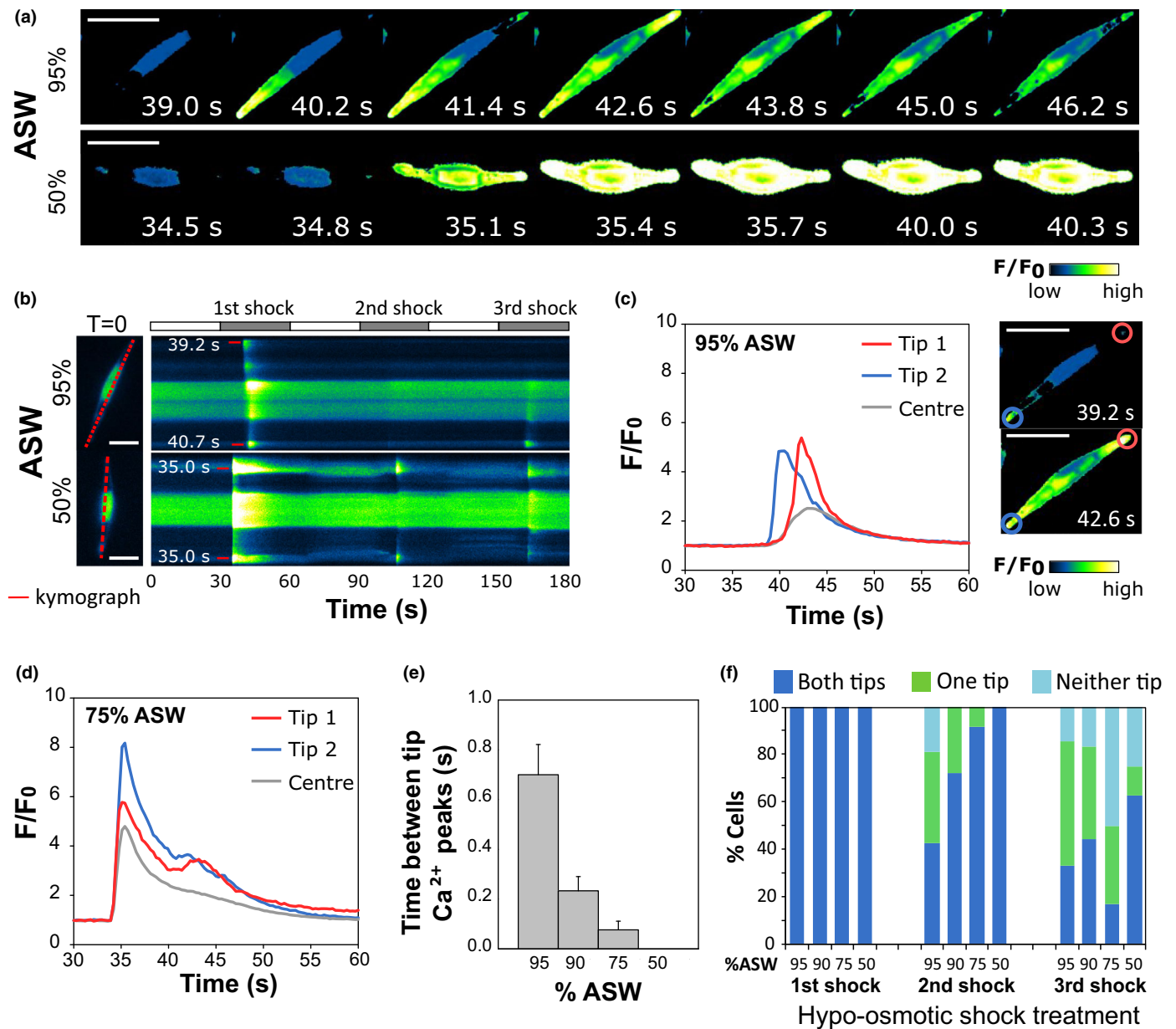


Fig. 2 Hypo-osmotic shock induces stimulus-strength specific spatial patterns of $[Ca^{2+}]_{cyt}$. (a) Pseudocoloured time-lapse images of fusiform PtR1 cells following perfusion with diluted ASW (95% ASW, top; 50% ASW, bottom). Time (s) after commencement of the experiment is indicated, when the hypo-osmotic shock was given after 30 s. Pseudocolour represents the change in fluorescence (F/F_0), indicating a rise in $[Ca^{2+}]_{cyt}$. Temporally separated Ca^{2+} waves that propagate from the apical cell tips are evident with milder (95% ASW) shocks. The initial blue signal represents chloroplast autofluorescence. Bars, 10 μ m. (b) Kymographs of representative cells (from (a)) exposed to three sequential 30 s hypo-osmotic shocks with 95% or 50% ASW. Hypo-osmotic shocks were given at 30, 90 and 150 s (grey bars) and between each shock cells were returned to standard ASW medium before the next treatment (white bars). The cell at $t = 0$ for each respective treatment is also shown, and a red line indicates how the kymograph was generated. The time (s) that the threshold F/F_0 value exceeded 1.15 for each tip is indicated for the first exposure to hypo-osmotic shock, for quantitative comparison (red arrows). Bars, 5 μ m. (c) Representative fluorescence traces (F/F_0) showing the timing and amplitude of the Ca^{2+} elevations in the cell tips (tip 1 and tip 2) vs the centre of the cell shown in (a) after exposure to 95% ASW. The traces indicate the change in F/F_0 of the tip regions and the centre of the cell during the initial hypo-osmotic shock, applied at 30 s for a duration of 30 s. The pseudocoloured images on the right correspond to the maximal amplitude in the two regions of interests (ROIs) at the tip of the cell, at 39.2 s (blue ROI) and 42.6 s (red ROI) respectively. Bars, 10 μ m. (d) Representative fluorescence traces (F/F_0) showing the timing and amplitude of the Ca^{2+} elevations in the cell tips (tip1 and tip 2) vs the centre of a cell exposed to 75% ASW. (e) Mean time between Ca^{2+} elevations in the tip regions during the initial hypo-osmotic shock. Cells that showed an elevation of 1.15 or above in both cell tips following first exposure to 30 s hypo-osmotic shock with 95%, 90% or 75% or 50% ASW were included (error bars indicate SEM; the experiments were repeated three times with a different sample of cells including a minimum of three cells in each independent sample, that is at least nine cells were examined in total for each treatment). Note that camera exposure was 300 ms. Timings represent difference between frames in which the Ca^{2+} elevations were detected. (f) Percentage of cells exposed to three sequential 30 s hypo-osmotic shocks with 95%, 90% or 75% or 50% ASW responding with either both, one or neither tips above a threshold F/F_0 of 1.15 or above.

strength dependent decoupling of cytosolic and nuclear Ca^{2+} compartments to hypo-osmotic stress: weaker osmotic shocks gave rise to smaller Ca^{2+} elevations that propagate from the tip region, whereas larger shocks resulted in substantial Ca^{2+} elevations across the whole cytosol and led to Ca^{2+} elevations that could be detected in the nucleus. These distinct patterns are likely to be important for governing different downstream responses.

Gradual decreases in osmolarity evoke repetitive $[\text{Ca}^{2+}]_{\text{cyt}}$ elevations

We have found that transient elevations in intracellular Ca^{2+} are evoked by rapid shifts in ASW dilution. However, natural diatom populations experience diverse osmotic regimes, from dramatic changes to more gradual decreases in osmolarity (Lewin & Guillard, 1963). Diatoms therefore need mechanisms to constantly monitor and adjust to incremental changes in osmolarity. To investigate whether and how hypo-osmotic- Ca^{2+} signals enable cells to detect more persistent gradual shifts in ASW dilution, that is whether Ca^{2+} elevations relate to the onset of hypo-osmotic stimuli or act to constantly monitor changes in osmolarity, we treated the PtR1 line to a ASW gradient using a gradient mixer. First, we exposed PtR1 cells to a steady decrease in osmolarity from 100% ASW to 75% ASW over 4 min. In this treatment, fusiform cells exhibited multiple, repetitive cytosolic Ca^{2+} elevations within 42.4 s (when the osmolarity reached *c.* 95% ASW), which continued for the duration of the treatment at a relatively uniform amplitude (Fig. 4a). Cells exhibited a maximum Ca^{2+} signal response in the tips of the cells. These elevations tended to propagate from the cell tip and, in many instances, occurred only in one tip (Fig. 4a, kymograph), suggesting that stress arising from the osmotic gradient is perceived locally rather than globally. Notably, repetitive elevations often alternated between tips. By contrast, exposure to a more severe gradient from 100% to 0% ASW caused a more rapid initial response within 9.5 ± 0.6 s (Fig. 4b), yet the threshold of osmolarity at which signalling initiated was at a similar range (96.1%). Moreover, these $[\text{Ca}^{2+}]_{\text{cyt}}$ spikes rarely returned to resting levels and had a higher frequency, although both the amplitude (Fig. 4c) and frequency of $[\text{Ca}^{2+}]_{\text{cyt}}$ spikes (Fig. 4d) attenuated over time. These data indicated that specific spatiotemporal patterns of hypo-osmotic-induced Ca^{2+} elevations within the cell also encoded important information about the nature of the environmental osmotic change. Ca^{2+} signals, therefore, not only arise following rapid shifts in osmotic conditions (via a single large Ca^{2+} elevation), but also enable continual sensing and adaptation to a dynamic osmotic environment through repetitive signalling events that differ in frequency and amplitude depending on the rate and/or extent of the change.

Oval cells exhibit a reduced sensitivity and enhanced tolerance to hypo-osmotic stress

P. tricornutum is pleomorphic, existing in different morphotypes in response to environmental conditions. These morphotypes include fusiform, triradiate and oval forms (De Martino *et al.*,

2011). Unlike the planktonic fusiform and triradiate forms, the oval morphotype typically grows in benthic biofilms, and is thus likely to encounter different osmotic gradients to planktonic cells. Moreover, hypo-osmotic stress is known to cause the CCAP1055/1 strain to transition from fusiform to oval morphotype (De Martino *et al.*, 2011). The experiments described above have focused on fusiform cells, and revealed that specific features of this cell morphotype (i.e. the apical tip regions) are particularly important for sensing hypo-osmotic shocks. We therefore investigated whether the different morphotypes have differing sensitivities and spatiotemporal patterns of Ca^{2+} signals in response to hypo-osmotic shock. Like fusiform cells, triradiate cells exhibited a Ca^{2+} wave that propagated from the cell tips following exposure to 95% ASW (3/3 cells) (Fig. 5a). However, very few oval morphotype cells exhibited an elevation in $[\text{Ca}^{2+}]_{\text{cyt}}$ with this treatment (2/18 cells compared with 30/31 fusiform cells) (Fig. 5b). Oval cells exposed to 90% ASW exhibited an elevation in $[\text{Ca}^{2+}]_{\text{cyt}}$, although there was no evidence for propagation from a localised region within the cell (Fig. 5c; Video S3). Importantly, control experiments treating oval morphotype PtR1-GFP cells to hypo-osmotic shock (with 60% ASW), did not cause changes in baseline GFP fluorescence, confirming that the observed increases in R-GECO1 fluorescence described were due to changes in cytosolic Ca^{2+} concentrations, rather than cell expansion artefacts (Fig. S4). Therefore, the reduced response of oval cells to 95% and 90% ASW compared with fusiform cells (Fig. 5b,d) suggested that this morphotype is less sensitive to subtle hypo-osmotic shocks. Indeed, whilst the average maximal increase in fluorescence (F/F_0) increased in a dose-dependent manner for the oval morphotype, it did not plateau with 50% and 25% ASW in contrast with fusiform cells (Fig. 5e). Furthermore, oval cells showed reduced responsiveness to fusiform cells when exposed to gradual changes in ASW (Fig. 5f,g). As triradiate cells only occur at very low frequencies in *P. tricornutum* strain CCAP/1055/1 (De Martino *et al.*, 2011) a full quantitative examination of the sensitivity of this morphotype was not possible. Nevertheless, these data demonstrated that the benthic oval morphology was less sensitive to hypo-osmotic stress, compared with planktonic fusiform cells, and may therefore be more resilient to fluctuating osmotic conditions.

Hypo-osmotic-induced decreases in organic osmolytes occur in a Ca^{2+} -independent manner

Our study highlights the widespread occurrence of hypo-osmotic Ca^{2+} signals, in different cellular compartments and to differing hypo-osmotic regimes. However, the specific roles of Ca^{2+} signalling in cellular acclimation to osmotic stress in diatoms remain unknown. Previous work has shown that external Ca^{2+} is necessary for hypo-osmotic-induced $[\text{Ca}^{2+}]_{\text{cyt}}$ elevations in *P. tricornutum* (Vardi *et al.*, 2006; Helliwell *et al.*, 2019). We therefore used the removal of Ca^{2+} as a tool to study the downstream consequences of hypo-osmotic shock, and examine whether such adjustments are dependent on Ca^{2+} . Proline, DMSP and GBT are the major organic osmolytes that accumulate in *P. tricornutum* under hyper-osmotic conditions (Schobert,

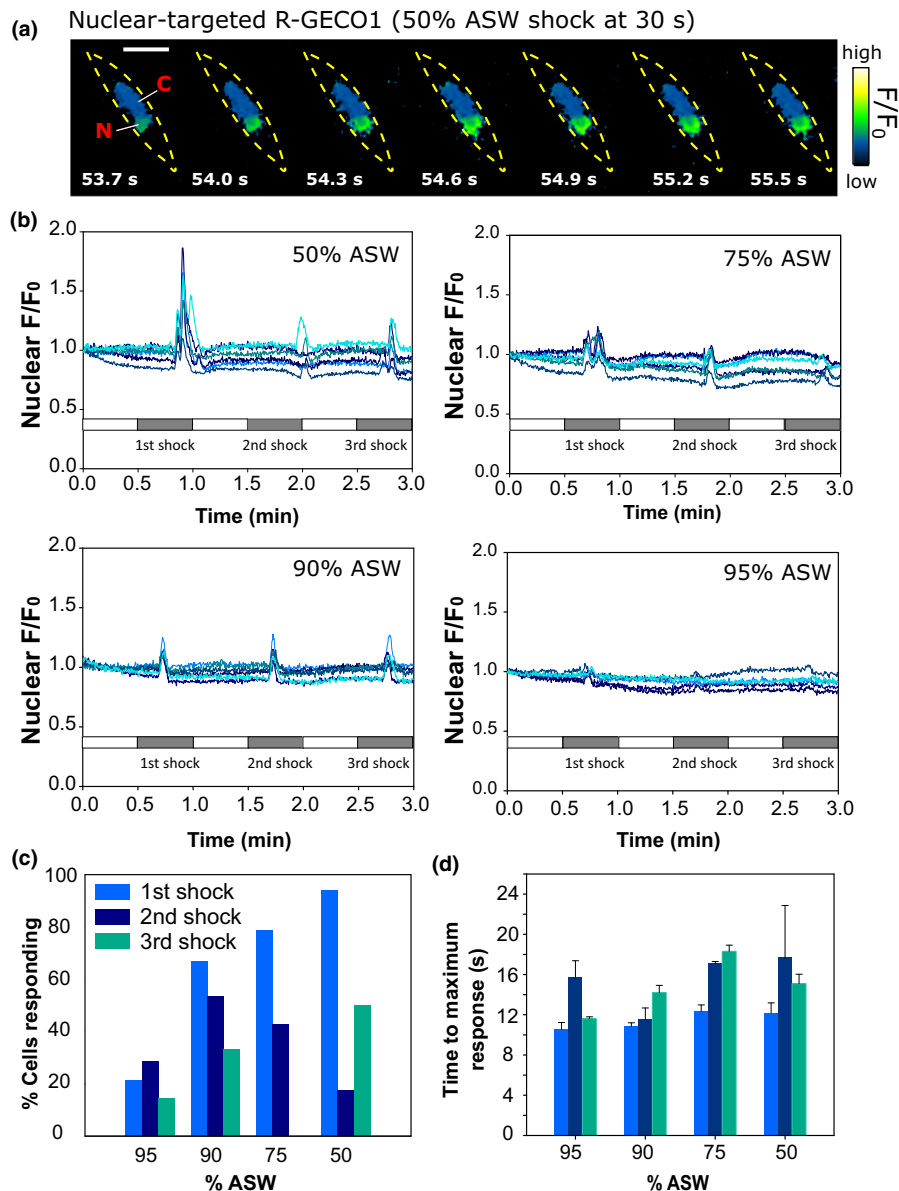


Fig. 3 Stimulus-strength specific nuclear Ca^{2+} signals in *Phaeodactylum tricornutum*. (a) Pseudocoloured time-lapse images of fusiform cell expressing nuclear-targeted R-GECO1 (Ptr1-N) following perfusion with diluted ASW (50%). Time (s) after commencement of the experiment is indicated, when the hypo-osmotic shock was given after 30 s. Pseudocolour represents the change in fluorescence (F / F_0), indicating a rise in $[\text{Ca}^{2+}]_{\text{nuc}}$. The chloroplast and nucleus are labelled 'c' and 'n', respectively, and the dashed yellow line indicates the cell boundary. Bars, 5 μm . (b) Representative traces of nuclear Ca^{2+} responses (F / F_0) over time for treatments with 50%, 75%, 90% or 95% ASW. Hypo-osmotic shocks were elicited at 30, 90 and 150 s (grey) and between each shock cells were returned to standard ASW medium (white) before the next treatment. Experiments were carried out on three independent occasions with similar results. (c) The percentage of cells expressing nuclear-targeted R-GECO1 that responded (above a threshold F / F_0 value of 1.15) to three sequential 30 s hypo-osmotic shocks with 95%, 90%, 75% or 50% ASW. (d) Mean time to maximum response (s) following successive hypo-osmotic shocks with ASW at a range of dilutions as described in (c). Data from the 1st shock, 2nd shock and 3rd shock are colour coded and labelled in the key shown in (c) (error bars: SEM, $n \geq 13$).

1980; Dickson & Kirst, 1987). It has previously been shown that proline is expelled during hypo-osmotic stress, with substantial decreases in intracellular concentrations detected when measured after 30 min (Schobert, 1980). To investigate whether Ca^{2+} elevations regulated the loss of these organic osmolytes, we quantified via HPLC-MS analysis concentrations of proline, DMSP and GBT in fusiform cells exposed to hypo-osmotic shock in the presence or absence of external Ca^{2+} . Notably, the intracellular

concentrations of proline, DMSP and GBT were the same in the control 'no-shock' treatment with or without Ca^{2+} , suggesting that the $-\text{Ca}^{2+}$ treatment did not cause solute loss due to impaired membrane integrity (Fig. 6a–c). However, we observed a significant decrease in intracellular concentrations of all three metabolites, following just 2 min treatments with 75% ASW, compared with the no-shock control (two-way ANOVA, $P < 0.001$ (proline and DMSP) and $P < 0.05$ (GBT)). Notably, a

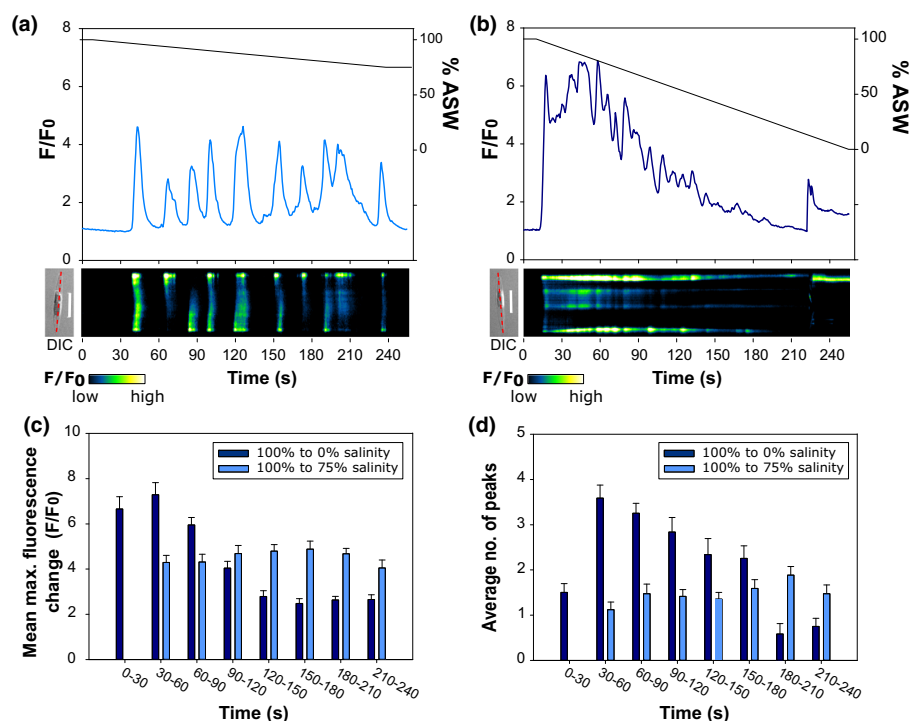


Fig. 4 Gradual decreases in osmolarity evoke repetitive $[Ca^{2+}]_{cyt}$ elevations in *Phaeodactylum tricornutum*. Representative trace of cytosolic Ca^{2+} response (F/F_0 , in which F_0 was an average of the first 16 frames) over time of a PtR1 cell exposed to gradual decreases in osmolarity from 100% to 75% ASW over a period of 4 min (0.11% decrease in salinity/second) (a), or 100% to 0% ASW (0.41% decrease in salinity/second) (b). Kymographs showing R-GECO1 fluorescence over time for each cell, as measured by epifluorescence microscopy, are displayed below each trace. A differential interference contrast (DIC) image of the cell examined for each respective treatment is shown, and the red dashed line indicates how the kymograph was generated (bar, 10 μ m). Similar responses were observed in $n = 16$ cells for each treatment, respectively. (c) Mean maximal fluorescence change (F/F_0) (within 30 s time intervals) of a population of cells ($n = 16$, error bars represent SEM) exposed to the different gradient treatments described in (a) and (b). (d) Average number of Ca^{2+} spikes (within 30 s time intervals) in cells exposed to the gradient treatments described in (a) and (b) (data are compiled from $n = 16$ cells, \pm SEM).

similar decrease was also observed in the $-Ca^{2+}$ treatment; no significant difference in osmolyte concentration was apparent between the different Ca^{2+} conditions (two-way ANOVA, $P > 0.2$). Together these data demonstrated that the rapid regulation of organic osmolytes following hypo-osmotic stress occurred in a Ca^{2+} -independent manner. NB: The slight reductions in intracellular concentrations on DMSP, GBT and proline in the 100% ASW treatment compared with the $t = 0$ control treatment, are likely to be due to loss of cells during the extra centrifugation step used in the treatment/harvesting of the 100% ASW treatment.

Hypo-osmotic-induced Ca^{2+} signals are required to prevent cell bursting

We have shown that hypo-osmotic-induced Ca^{2+} elevations do not control the efflux of key organic osmolytes. We therefore determined if osmotic-induced Ca^{2+} signals were important for maintaining cell health more broadly. We found that treatment with 75% ASW $-CaCl_2$ (+200 μ M EGTA) had no obvious damaging effect on cell integrity (Fig. 7a). However, a substantial increase in cell area, which far exceeded that seen in the $+Ca^{2+}$ (standard ASW) treatment was apparent (Fig. 7b). This indicated a Ca^{2+} -dependent regulation of cell expansion, and suggested that the Ca^{2+} -independent loss of organic osmolytes could not

prevent cell expansion during hypo-osmotic shock. This effect was most severe with stronger shocks. Exposure of fusiform cells to 50% ASW without $CaCl_2$ (+200 μ M EGTA) caused bursting in 11% of cells (Fig. 7c). However, the 25% ASW treatment without Ca^{2+} (+200 μ M EGTA), led to cell bursting in 91% of cells, compared with 4.8% of cells in the presence of Ca^{2+} (standard ASW) (Fig. 7c). We found that treatment of cells to a ASW gradient $-CaCl_2$ also led to cell bursting in 97.4% cells (Fig. 7d), unlike in the presence of external Ca^{2+} (in which 0/11 cells burst) (Fig. 7e). Therefore, hypo-osmotic-induced Ca^{2+} signals are critical for maintaining cell volume and integrity. Notably, this effect was less pronounced in oval morphotype cells: only 43.8% burst following exposure to 25% ASW $-CaCl_2$ (compared with 91% in the fusiform treatment) (Fig. 7c), consistent with the hypothesis that this morphotype is more resilient to osmotic shock.

As removing Ca^{2+} from the medium could potentially have indirect effects on the exterior of the cell, for example influencing cell wall integrity, we also examined whether Ca^{2+} was required for volume regulation internally. In eukaryotes, cell volume regulation requires coordinated changes between the plasma and vacuolar membrane (Matile, 1978; Shabala & Lew, 2002). To examine, *in situ* changes to vacuole architecture we stained cells with the tonoplast stain MDY-64 (Huang *et al.*, 2016). We observed that MDY-64 stained *P. tricornutum* cells exhibited two large vacuoles either side of the central cytoplasmic region

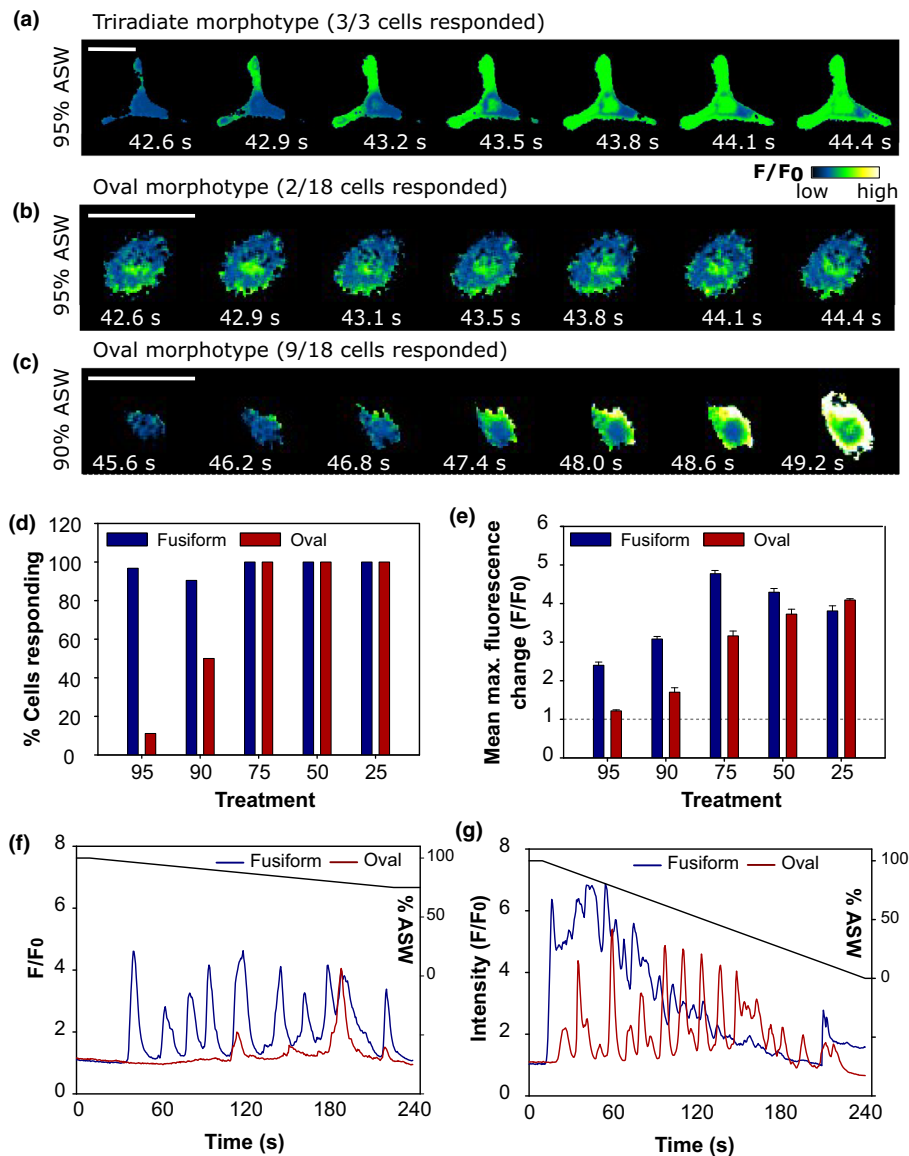


Fig. 5 Benthic oval *Phaeodactylum tricornutum* morphotype exhibits reduced sensitivity to subtle hypo-osmotic shocks compared with planktonic fusiform and triradiate cells. Ca^{2+} imaging using R-GECO1 *P. tricornutum* Ptr1 strain, displaying pseudocoloured time-lapse images of representative triradiate (a) and oval (b) cells following perfusion with 95% ASW. An oval cell treated with 90% ASW is also shown (c). Bars, 10 μm . The total number of cells that displayed a $[Ca^{2+}]_{cyt}$ elevation > 1.15 (over the number of cells examined in total), for (a–c) is indicated in parentheses. (d) Percentage of oval cells exhibiting a $[Ca^{2+}]_{cyt}$ elevation > 1.15 to hypo-osmotic shocks with ASW at a range of dilutions. The % of fusiform cells responding (exposed to the same treatments), as previously described in Fig. 1e are also shown, for comparison. Data collated from three independent replicate experiments per line and a minimum of $n = 13$ cells were examined in total per treatment. (e) Mean maximal fluorescence change (F/F_0) of oval and fusiform cells exposed to hypo-osmotic shocks with ASW at a range of dilutions. Data collated from three independent replicate experiments (error bars: SEM). Only cells that exhibited a $[Ca^{2+}]_{cyt}$ elevation (above F/F_0 threshold of 1.15) were included, and a minimum total of $n = 13$ cells were examined per treatment. Baseline fluorescence (i.e. $F/F_0 = 1$) is indicated with a dashed grey line. (f, g) Representative trace of $[Ca^{2+}]_{cyt}$ response (F/F_0 in which F_0 represents an average of the first 16 frames for this experiment) over time of an oval Ptr1 cell exposed to gradual decreases in osmolarity from 100% to 75% ASW over a period of 4 min (0.11% decrease in salinity/second) (f), or 100% to 0% ASW (0.41% decrease in salinity/second) (g), compared with a fusiform cell grown under the same conditions (as shown previously in Fig. 4a,b).

containing the nucleus and the chloroplast, as is typically observed in this species (Huang *et al.*, 2016) (yellow labelling, Fig. 7f). Treatment of stained fusiform cells with 50% ASW for 60 s caused a slight tonoplast rearrangement including the appearance of small vacuoles (Fig. 7g, red arrows), but in general the two large vacuole structures remained intact (9.1% cells

showed tonoplast rupture (as defined in the Methods)). In the absence of extracellular Ca^{2+} (+200 μM EGTA) the rearrangement was more pronounced, with clear tonoplast rupture in 64% of cells (Fig. 7g). This finding suggested that removing Ca^{2+} affected cell bursting primarily through the inhibition of $[Ca^{2+}]_{cyt}$ elevations, rather than an indirect effect on cell wall

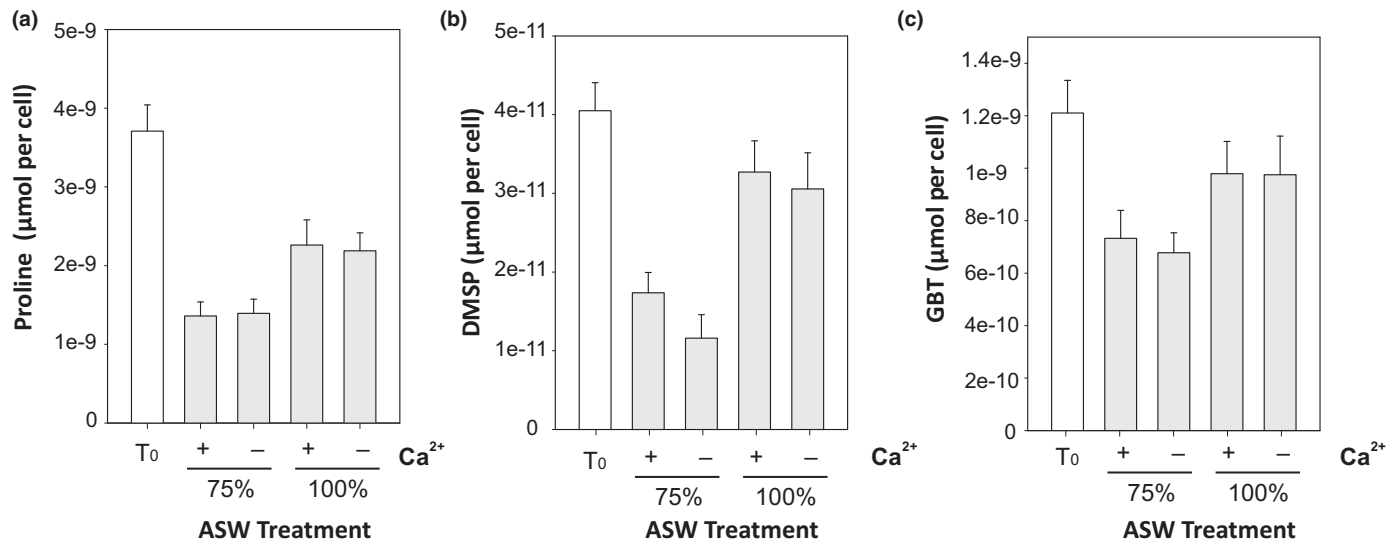


Fig. 6 Rapid decreases of organic osmolytes occur in a Ca^{2+} -independent manner. Intracellular concentrations of (a) proline, (b) DMSP and (c) glycine betaine (GBT) in response to different 2 min hypo-osmotic shock treatments with or without Ca^{2+} . For this, cells were treated with ASW (i.e. with 10 mM CaCl_2) (+) or ASW without Ca^{2+} + 200 μM EGTA (–) diluted to 75% (75% treatment) or undiluted (100% treatment). For treatments without Ca^{2+} , 200 μM EGTA was added (see the Materials and Methods section). Data are means \pm SEM ($n = 5$). Two-way ANOVA analyses (with a Holm–Sidak post hoc test) determined that, in all instances, a significant difference in osmolyte concentration was observed in the shock (75% ASW) vs no-shock (100% ASW) treatment: $P < 0.001$ (proline and DMSP) and $P < 0.05$ (GBT). By contrast, the presence/absence of Ca^{2+} did not have a significant effect.

integrity, for example. Together, these results demonstrated that hypo-osmotic-induced Ca^{2+} signals are essential for coordinated cell and vacuolar volume regulation and survival. Moreover, the data indicated that Ca^{2+} -independent efflux of organic osmolytes was not sufficient to withstand the damaging consequences of osmotic shock to cell integrity.

Ca^{2+} -signalling is necessary to coordinate K^+ efflux during hypo-osmotic shock

In *P. tricornutum*, the osmotic balance is maintained by coordination of organic osmolytes, and inorganic ions (predominantly K^+) (Dickson & Kirst, 1987). Certainly, steady-state intracellular concentrations of K^+ increase in *P. tricornutum* cells grown at elevated salinities (Dickson & Kirst, 1987). To investigate real-time intracellular K^+ concentrations in response to hypo-osmotic shock in single *P. tricornutum* cells, we developed a transgenic line expressing the genetically encoded K^+ biosensor (GINKO1) (Shen *et al.*, 2018). However, although we detected changes in GINKO1 fluorescence intensity in response to hypo-osmotic shock (Fig. S5a), our interpretation of these results was hindered by the substantial pH sensitivity of this eGFP-based biosensor (Fig. S5b). As cytosolic Ca^{2+} elevations are closely associated with changes in pH in plant cells (Behera *et al.*, 2018), we sought alternative methods to measure K^+ transport, using fabricated K^+ -selective microelectrodes.

We measured changes in extracellular K^+ concentration in dense cultures of *P. tricornutum*, exposed to a 75% ASW shock. Addition of ddH₂O to induce hypo-osmotic shock (by lowering the salinity from 100% ASW to 75% ASW) would lead to a dilution in the K^+ concentration in ASW from 10 mM to 7.5 mM. However, any release of intracellular K^+ by the cells during the

shock would result in a smaller decrease in external K^+ concentration. In this regard, we saw a rapid reduction in extracellular K^+ concentration in cell suspensions following addition of ddH₂O to the culture (Fig. 8a). However, the reduction in external $[\text{K}^+]$ (measured from immediately before the shock to 30 s after the shock) was significantly lower in the presence of Ca^{2+} compared with cells in the absence of external Ca^{2+} (+100 μM EGTA) ($n = 16$ and 13 independent treatments, respectively) (Fig. 8a). Furthermore, the $\Delta[\text{K}^+]$ in the absence of external Ca^{2+} (+100 μM EGTA) was very similar to the value expected if no K^+ efflux occurred during hypo-osmotic shock (mean $\Delta[\text{K}^+] = -2.42 \pm 0.27 \text{ mM}$) (Fig. 8b). These experiments strongly suggested that rapid K^+ efflux occurred during hypo-osmotic shock in *P. tricornutum* and that Ca^{2+} signals played a direct role in regulating this process.

Discussion

Diatoms encounter dynamic and severe fluctuations in osmotic conditions over diverse spatiotemporal scales. Metabolic attributes enabling these important phytoplankton to sense and rapidly acclimate to rapid osmotic shifts are therefore critical to their ecological success. We have applied novel single-cell imaging approaches, coupled with osmolyte analysis, to gain new insights into the dynamic real-time responses of *P. tricornutum* cells to hypo-osmotic stress. Our results demonstrated that distinct spatiotemporal patterns of intracellular Ca^{2+} encode important information regarding osmotic change, such as severity and temporal features of the environmental stimuli. We found that localised Ca^{2+} signals evoked by mild or gradual shifts in % ASW were propagated globally from the apical cell tips, enabling precise cell volume regulation across the whole cell. Importantly,

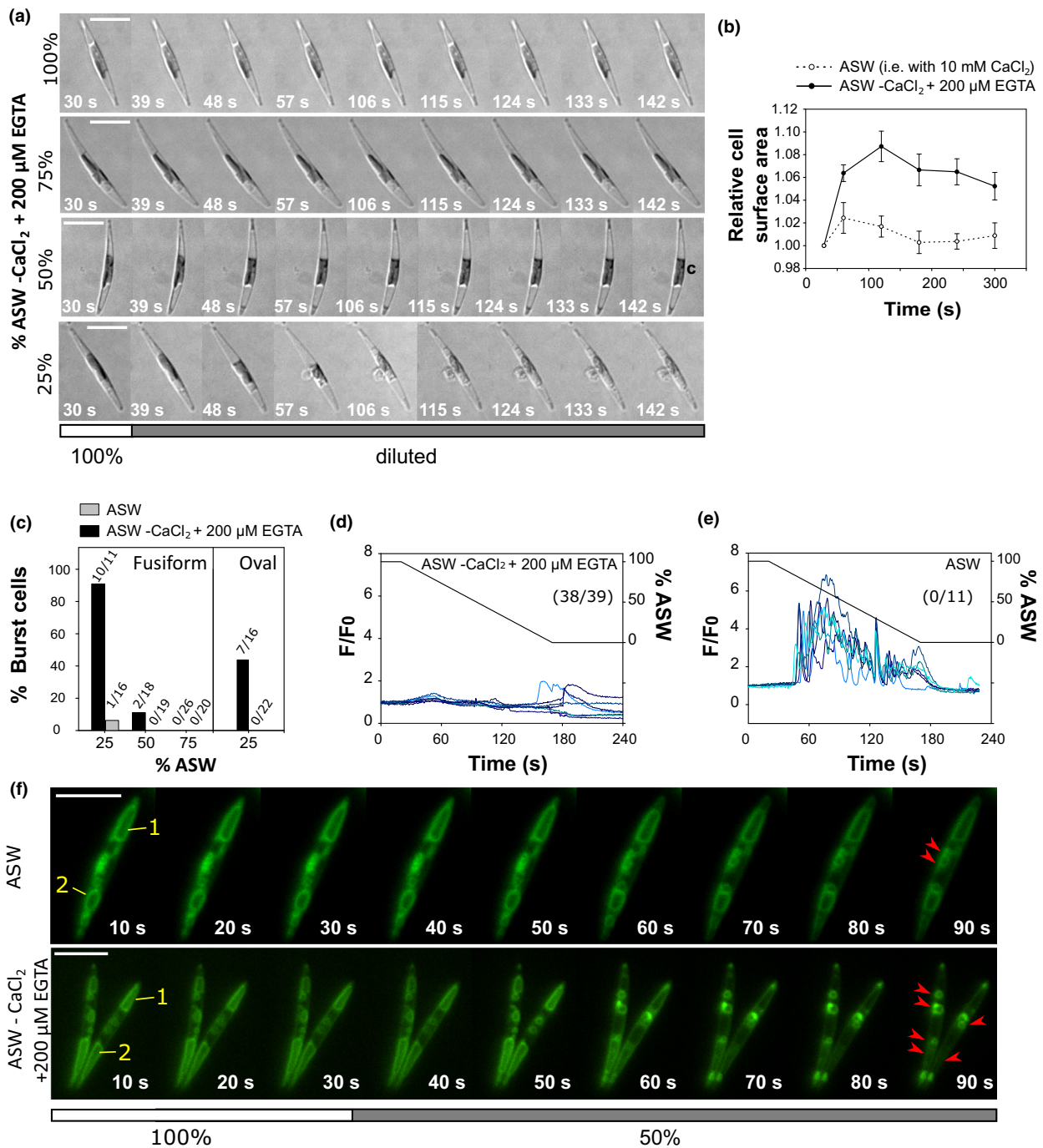


Fig. 7 Ca²⁺-dependent signalling is required for cell volume regulation to prevent cell bursting in *Phaeodactylum tricornutum*. (a) Live-cell DIC video microscopy of fusiform *P. tricornutum* cells exposed to ASW -Ca²⁺ + 200 μM EGTA diluted to 75%, 50% and 25%, or undiluted (100%). Bars, 10 μm. (b) Changes in cell surface area, relative to preshock values of cells exposed to 75% ASW vs 75% ASW made up without CaCl₂ (for the ASW -Ca²⁺ medium, 200 μM EGTA was added (see the Materials and Methods section)). In total, *n* = 9 cells over three independent replicate experiments were examined (error bars denote SEM). (c) The percentage of fusiform and oval cells that bursts during exposure to hypo-osmotic shocks in ASW or ASW without CaCl₂ in the medium (+200 μM EGTA in the ASW -Ca²⁺ medium) (see the Materials and Methods section). The number of burst cells/the number of cells examined in total of three independent experiments is also given for each treatment. (d, e) [Ca²⁺]_{cyt} response (*F* / *F*₀) over time of fusiform PtR1 cells exposed to ASW gradient from 100% to 0% ASW over a period of 240 s (0.67% decrease in salinity/second) either without (d) or with Ca²⁺ (e) in the perfusion medium. The number of cells that burst/total number of cells, is shown in parentheses. (f) Vacuolar membrane (MDY-64) stained cells exposed to 50% ASW or 50% ASW without CaCl₂ (+200 μM EGTA in the ASW -Ca²⁺ medium) (see the Materials and Methods section). The two large vacuoles either side of the central cytoplasmic region containing the nucleus and chloroplast, as typically reported in *P. tricornutum* cells (Huang *et al.*, 2016), are labelled '1' and '2' in yellow. Bars, 10 μm. In total, *n* = 11 cells were examined over three independent replicate experiments per treatment. Rearrangements in tonoplast structure, including the appearance of small vacuoles and/or fragmentation of the larger vacuoles into smaller vacuoles are highlighted with red arrows.

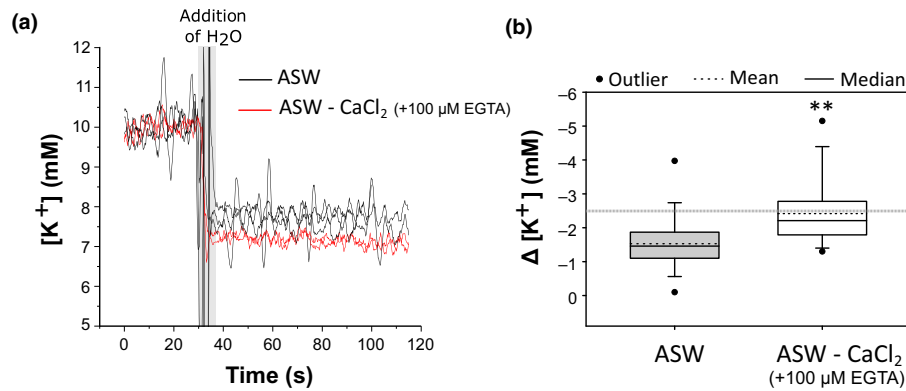


Fig. 8 Ca^{2+} -dependent signalling is necessary to coordinate K^{+} efflux during hypo-osmotic shock. (a) Representative traces of K^{+} concentration in a suspension of *Phaeodactylum tricornutum* cells in ASW being exposed to a hypo-osmotic shock with diluted ASW or diluted ASW made up without CaCl_2 (+100 μM EGTA for the $-\text{Ca}^{2+}$ treatment). ddH_2O was added at 30 s to lower salinity from 100% ASW to 75% ASW, resulting in a change in external K^{+} from 10 mM to 7.5 mM in the absence of any biological activity. The shaded area indicates electrode noise caused by the addition of ddH_2O to the cell suspension. (b) The change in K^{+} concentration ($\Delta[\text{K}^{+}]$ in mM) post hypo-osmotic shock (30 s) in ASW vs ASW $-\text{CaCl}_2$ (+100 μM EGTA) (see the Materials and Methods section) for the experiments described in (a). Data represent mean \pm SD, and is compiled from $n = 16$ and $n = 13$ independent treatments, for $+\text{Ca}^{2+}$ and $-\text{Ca}^{2+}$ (+100 μM EGTA) treatments, respectively. **The difference between ASW and ASW- CaCl_2 (+100 μM EGTA) treatments was significantly different (Student's t -test, $P < 0.01$). The expected $\Delta[\text{K}^{+}]$ due to the addition of ddH_2O (i.e. 2.5 mM) is indicated by the broken grey line. NB: For the experiments displayed in this figure the concentration of K^{+} in the ASW medium was 10 mM.

hypo-osmotic-induced Ca^{2+} signals were essential for maintaining cell integrity and prevented ultrastructural damage. Characterisation of rapid physiological adaptations to hypo-osmotic shocks, and examination of their Ca^{2+} dependency, led us to identify Ca^{2+} -dependent and Ca^{2+} -independent mechanisms for early osmoregulation (Fig. 9). We found that efflux of organic osmolytes (including proline, DMSP and glycine betaine) occurred within minutes following hypo-osmotic shock, but were detected even in the absence of external Ca^{2+} , and were not sufficient to prevent cell bursting. By comparison, hypo-osmotic-induced Ca^{2+} signals were necessary for precise and rapid coordination of K^{+} content, which is likely to be responsible for the immediate Ca^{2+} -dependent regulation of cell volume observed during acute hypo-osmotic stress. Together our findings allowed us propose an advanced model for *P. tricornutum* osmoregulation (Fig. 9) and demonstrate that the hypo-osmotic Ca^{2+} signalling pathway is likely to be critical to diatom survival in dynamic osmotic environments.

The role for Ca^{2+} signalling for sensing hypo-osmotic shock appears to be universally conserved in eukaryotes, including across animals, fungi, plants, green algae, brown seaweeds and diatoms (Takahashi *et al.*, 1997; Cessna *et al.*, 1998; Falcioro *et al.*, 2000; Goddard *et al.*, 2000; Bickerton *et al.*, 2016). In animal and fungal cells, cell volume alterations following hypo-osmotic shock are coupled to several osmotic-signalling responses that coordinate regulatory volume decrease (RVD) (Hoffmann *et al.*, 2009). Activation of mechanosensitive and/or osmosensitive channels causes a transient increase in intracellular Ca^{2+} . Several members of the transient receptor potential (TRP) subfamily of cation channels are activated by osmotic stimuli and/or contribute to the volume regulatory response in animals (Hoffmann *et al.*, 2009). In yeast (*Saccharomyces cerevisiae*), two mechanosensitive channels (Msy1 and Msy2) have been identified to be involved in cell volume regulation following hypo-osmotic shock. Likewise, the mechanosensitive channel MSL10 was recently

demonstrated to potentiate responses to hypo-osmotic shock in *Arabidopsis thaliana* (Basu & Haswell, 2020). *P. tricornutum* encodes a suite of channels resembling mechanosensitive/stretch-activated channels (including seven small conductance mechanosensitive channels (MscS) and four TRP channels) (Verret *et al.*, 2010). Additionally, this species also encodes OSCA channels, representatives of which have also been shown to be mechanosensitive channels that are important for osmo-sensing in *A. thaliana* (Yuan *et al.*, 2014; Murthy *et al.*, 2018; Zhang *et al.*, 2018). This raises the possibility that one or more of these channels may be involved in generating cytosolic Ca^{2+} elevations. However, further work is necessary to deduce the specific channel (s) that initiate rapid hypo-osmotic-induced Ca^{2+} signals, which are clearly vital for enduring stressful downshifts in osmolarity.

Our experiments also clearly demonstrated that fusiform and triradiate *P. tricornutum* cells exhibited fast $[\text{Ca}^{2+}]_{\text{cyt}}$ waves in response to subtle hypo-osmotic shocks. The speed of *P. tricornutum* Ca^{2+} waves ($37.11 \mu\text{m s}^{-1} \pm 5.97$) are not dissimilar from those documented in animal cells (Jaffe, 2010) that are generated by Ca^{2+} -dependent activation of ER-localised inositol triphosphate receptors (IP_3Rs) (Supattapone *et al.*, 1988). There is evidence for *in vivo* IP_3 -induced Ca^{2+} release in plants, pointing to the significance of IP_3 signalling outside the Opisthokonta (Krinke *et al.*, 2006). However, no plant IP_3R has been identified so far, and *P. tricornutum* does not encode IP_3R (Verret *et al.*, 2010). The specific roles and mechanisms for Ca^{2+} -induced Ca^{2+} release in diatoms clearly warrant future investigation.

Notably, the cytosolic Ca^{2+} waves of *P. tricornutum* were confined to milder shocks. Thus, whilst subtle osmotic changes may be perceived locally, this localised primary signal can then be propagated more broadly, to enable global cellular responses. Moreover, these stimulus-specific Ca^{2+} signals encode important information about the nature of the osmotic change. This was particularly appropriate in light of our evidence that nuclear Ca^{2+} signals were only detected in *P. tricornutum* in response to severe

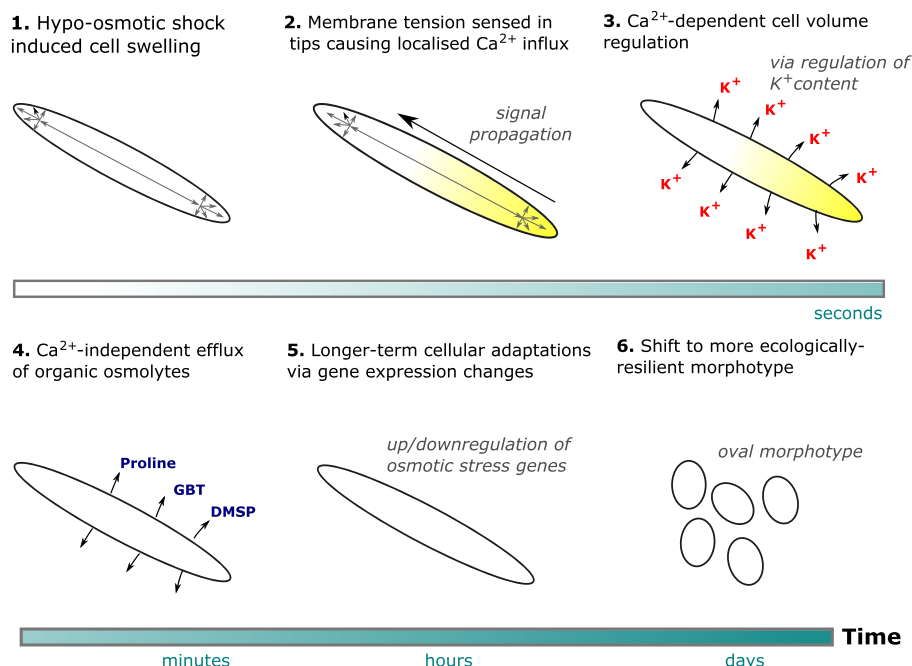


Fig. 9 Model for hypo-osmotic shock regulation in *Phaeodactylum tricornutum*. Schematic diagram of the cellular processes coordinating short-, medium- and long-term acclimation responses to hypo-osmotic stress in *P. tricornutum*, via Ca^{2+} -dependent and Ca^{2+} -independent mechanisms.

hypo-osmotic shock, compared with cytosolic Ca^{2+} elevations, which were evoked even with very mild treatments. Whilst it is possible that the small volume of the nucleus may influence our ability to detect nuclear Ca^{2+} elevations, our results pointed to a decoupling of Ca^{2+} signalling in the cytosolic and nuclear compartments that could lead to alternative outputs in gene expression to distinct osmotic stimuli (Bootman *et al.*, 2009; Stael *et al.*, 2012). Moreover, the fact that Ca^{2+} wave propagation initiates in the cell tip(s) suggests that this part of the cell may function as a hypersensitive micro-sensor/antenna. Whether this is due to regional channel localisation, or because cell expansion exerts the greatest forces on the apical tips, remains to be elucidated. Certainly, evidence of regional cation channel localisation, has emerged from other systems (Korchev *et al.*, 2000), with important functional implications.

Key acclimation responses of diatoms to mitigate the harmful consequences of hypo-osmotic shock include critical short-term adjustments in inorganic ions (namely K^{+} (Dickson & Kirst, 1987)) to control immediate changes in cell volume, and regulation of organic osmolytes. Longer-term changes in gene expression occur subsequently (De Martino *et al.*, 2011), and could be a consequence of $[\text{Ca}^{2+}]_{\text{nuc}}$ elevations. In animal cells, rapid RVD is mediated by two major ion efflux mechanisms: (1) swell-activated anion (carried by Cl^{-} ions and organic osmolytes), and (2) cation (K^{+}) channels. The volume-regulated anion current is fully Ca^{2+} independent in animals (Hoffmann & Pedersen, 2011). Several types of swell-activated K^{+} channels are also implicated, and at least some of these are Ca^{2+} dependent (Hoffmann *et al.*, 2009). We found evidence for Ca^{2+} -independent regulation of organic osmolytes efflux in *P. tricornutum*. By comparison, we reported that extracellular Ca^{2+} is necessary for

mediating K^{+} transport in response to hypo-osmotic shock in *P. tricornutum*. In particular, using K^{+} -selective microelectrodes, we demonstrated that *P. tricornutum* cells suspended in ASW rapidly released K^{+} upon hypo-osmotic shock (to 75% ASW), but that this response was inhibited in the absence of external Ca^{2+} (+100 μM EGTA). Therefore, Ca^{2+} -dependent regulation of K^{+} efflux for example through Ca^{2+} -regulated K^{+} channels, is likely to be involved in mediating this important protective response. As an aside, our study also demonstrated the pH sensitivity of the genetically encoded K^{+} -sensitive fluorescent probe, GINKO1 (Shen *et al.*, 2019), cautioning its use as a reliable K^{+} indicator without simultaneous examination of intracellular pH.

Finally, our work demonstrated that these Ca^{2+} -dependent responses are essential for the ecological tolerance of diatoms to withstand hostile osmotic conditions, as removal of the external Ca^{2+} leads to cell bursting. These signalling mechanisms therefore are likely to underpin the ability of diatoms to colonise estuaries and sea-ice environments. These findings, coupled with recent evidence that diatoms employ Ca^{2+} -dependent signalling mechanisms for nutrient (phosphate) sensing (Helliwell *et al.*, 2020), underline the important role of Ca^{2+} signalling for diatom environmental perception. The adoption of distinct mechanisms for osmoregulation in diatoms, controlled by different Ca^{2+} -dependent and Ca^{2+} -independent regulatory pathways, may be a necessary ecological strategy to minimise the unnecessary loss of costly organic metabolites. These two mechanisms may also occur over different timescales to facilitate short-term and medium-term adaptations (Fig. 9). Going forward, the elucidation of specific molecular components of the osmotic Ca^{2+} -signalling pathway will allow a greater understanding of how Ca^{2+} -dependent and Ca^{2+} -independent responses are coordinated to

enhance ecological competitiveness of diatoms in highly dynamic aquatic ecosystems.




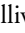

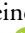


Acknowledgements

We acknowledge support from the European Research Council, grant ERC-ADG-670390 (CB), and NERC Independent Research Fellowship grant NE/R015449/2 (KEH). The authors declare no conflicting interests.

Author contributions

KEH, GLW and CB designed the research. KEH, FHK, CB and AC performed experiments. KEH, FHK, DS, CB and GLW carried out data analysis. KEH, FHK, GLW, NS, CB interpreted the data. KEH, HH and TG generated materials and strains for the research. KEH wrote the manuscript, with feedback from GLW, CB and FHK.

ORCID

Colin Brownlee  <https://orcid.org/0000-0001-7838-230X>
 Abdul Chrchri  <https://orcid.org/0000-0002-6223-6049>
 Trupti Gaikwad  <https://orcid.org/0000-0001-7271-211X>
 Katherine E. Helliwell  <https://orcid.org/0000-0002-2068-576X>
 Friedrich H. Kleiner  <https://orcid.org/0000-0002-8429-0636>
 Deborah Salmon  <https://orcid.org/0000-0002-5270-358X>
 Nicholas Smirnoff  <https://orcid.org/0000-0001-5630-5602>
 Glen L. Wheeler  <https://orcid.org/0000-0002-4657-1701>

References

- Armbrust EV. 2009. The life of diatoms in the world's oceans. *Nature* 459: 185–192.
- Balzano S, Sarno D, Kooistra WHCF. 2011. Effects of salinity on the growth rate and morphology of ten *Skeletonema* strains. *Journal of Plankton Research* 33: 937–945.
- Basu D, Haswell ES. 2020. The mechanosensitive ion channel MSL10 potentiates responses to cell swelling in *Arabidopsis* seedlings. *Current Biology* 30: 2716–2728.
- Behera S, Xu Z, Luoni L, Bonza MC, Doccula FG, De Michelis MI, Morris RJ, Schwarzländer M, Costa A. 2018. Cellular Ca^{2+} signals generate defined pH signatures in plants. *The Plant Cell* 30: 2704–2719.
- Bickerton P, Sello S, Brownlee C, Pittman JK, Wheeler GL. 2016. Spatial and temporal specificity of Ca^{2+} signalling in *Chlamydomonas reinhardtii* in response to osmotic stress. *New Phytologist* 212: 920–933.
- Bootman MD, Fearnley C, Smyrniak I, MacDonald F, Roderick HL. 2009. An update on nuclear calcium signalling. *Journal of Cell Science* 122: 2337–2350.
- Cessna SG, Chandra S, Low PS. 1998. Hypo-osmotic shock of tobacco cells stimulates Ca^{2+} fluxes deriving first from external and then internal Ca^{2+} stores. *The Journal of Biological Chemistry* 273: 27286–27291.
- De Martino A, Bartual A, Willis A, Meichenin A, Villazán B, Maheswari U, Bowler C. 2011. Physiological and molecular evidence that environmental changes elicit morphological Interconversion in the model diatom *Phaeodactylum tricornutum*. *Protist* 162: 462–481.
- Dickson DMJ, Kirst GO. 1987. Osmotic adjustment in marine eukaryotic algae: the role of inorganic ions, quaternary ammonium, tertiary sulphonium and carbohydrate solutes. I. Diatoms and a rhodophyte. *New Phytologist* 106: 645–655.
- Edel KH, Marchadier E, Brownlee C, Kudla J, Hetherington AM. 2017. The evolution of calcium-based signalling in plants. *Current Biology* 27: R667–R679.
- Falciatore A, D'Alcalá MR, Croot P, Bowler C. 2000. Perception of environmental signals by a marine diatom. *Science* 288: 2363–2366.
- Falkowski PG, Katz ME, Knoll AH, Quigg A, Raven JA, Schofield O, Taylor FJR. 2004. The evolution of modern eukaryotic phytoplankton. *Science* 305: 354–360.
- Francius G, Tesson B, Dague E, Martin-Jézéquel V, Dufrène YF. 2008. Nanostructure and nanomechanics of live *Phaeodactylum tricornutum* morphotypes. *Environmental Microbiology* 10: 1344–1356.
- Garza-Sánchez F, Chapman DJ, Cooper JB. 2009. *Nitzschia ovalis* (Bacillariophyceae) mono lake strain accumulates 1,4/2,5 cyclohexanetetrol in response to increased salinity. *Journal of Phycology* 45: 395–403.
- Goddard H, Manison NF, Tomos D, Brownlee C. 2000. Elemental propagation of calcium signals in response-specific patterns determined by environmental stimulus strength. *Proceedings of the National Academy of Sciences, USA* 97: 1932–1937.
- Guillard RRL. 1975. Culture of phytoplankton for feeding marine invertebrates. In: Smith WL, Chanley MH, eds. *Culture of marine invertebrate animals*. Boston, MA, USA: Springer, 29–60.
- Guillard RRL, Ryther JH. 1962. Studies of marine planktonic diatoms. I. *Cyclotella nana* Hustedt, and *Detonula confervacea* (Cleve) Gran. *Canadian Journal of Microbiology* 8: 229–239.
- Helliwell KE, Chrchri A, Koester JA, Wharam S, Verret F, Taylor AR, Wheeler GL, Brownlee C. 2019. Alternative mechanisms for fast $\text{Na}^+/\text{Ca}^{2+}$ signaling in eukaryotes via a novel class of single-domain voltage-gated channels. *Current Biology* 29: 1503–1511.
- Helliwell KE, Harrison E, Christae-Oleza J, Rees A, Kleiner F, Gaikwad T, Downe J, Ferretjans M, Al-Moosawi L, Brownlee C *et al.* 2020. A novel Ca^{2+} signalling pathway co-ordinates environmental phosphorus sensing and nitrogen metabolism in marine diatoms. *Current Biology* 31: 1–12.
- Hoffmann EK, Lambert IH, Pedersen SF. 2009. Physiology of cell volume regulation in vertebrates. *Physiological Reviews* 89: 193–277.
- Hoffmann EK, Pedersen SF. 2011. Cell volume homeostatic mechanisms: effectors and signalling pathways. *Acta Physiologica* 202: 465–485.
- Huang F, Luo J, Ning T, Cao W, Jin X, Zhao H, Wang Y, Han S. 2017. Cytosolic and nucleosolic calcium signaling in response to osmotic and salt stresses are independent of each other in roots of *Arabidopsis* seedlings. *Frontiers in Plant Science* 8: 1648.
- Huang W, Río Bártulos C, Kroth PG. 2016. Diatom vacuolar 1,6- β -transglycosylases can functionally complement the respective yeast mutants. *Journal of Eukaryotic Microbiology* 63: 536–546.
- Jaffe LF. 2010. Fast calcium waves. *Cell Calcium* 48: 102–113.
- Keinath NF, Waadt R, Brugman R, Schroeder JI, Grossmann G, Schumacher K, Krebs M. 2015. Live cell imaging with R-GECO1 sheds light on *flg22*- and chitin-induced transient $[\text{Ca}^{2+}]_{\text{cyt}}$ patterns in *Arabidopsis*. *Molecular Plant* 8: 1188–1200.
- Kirst GO. 1990. Salinity tolerance of eukaryotic marine algae. *Annual Review of Plant Physiology and Plant Molecular Biology* 41: 21–53.
- Korchev YE, Negulyaev YA, Edwards CRW, Vodyanoy I, Lab MJ. 2000. Functional localization of single active ion channels on the surface of a living cell. *Nature Cell Biology* 2: 616–619.
- Krell A, Funck D, Plettner I, John U, Dieckmann G. 2007. Regulation of proline metabolism under salt stress in the psychrophilic diatom *Fragilariopsis cylindrus* (Bacillariophyceae). *Journal of Phycology* 43: 753–762.
- Krinke O, Novotna Z, Valentova O, Martinec J. 2006. Inositol triphosphate receptor in higher plants: is it real? *Journal of Experimental Botany* 58: 361–376.
- Lewin JC, Guillard RRL. 1963. Diatoms. *Annual Review of Microbiology* 17: 373–414.
- Matile P. 1978. Biochemistry and function of vacuoles. *Annual Review of Plant Physiology* 29: 193–213.
- Murthy SE, Dubin AE, Whitwam T, Jojoa-Cruz S, Cahalan SM, Mousavi SAR, Ward AB, Patapoutian A. 2018. OSCA/TMEM63 are an evolutionarily conserved family of mechanically activated ion channels. *eLife* 7: e41844.
- Nakayama Y, Yoshimura K, Iida H. 2012. Organellar mechanosensitive channels in fission yeast regulate the hypo-osmotic shock response. *Nature Communications* 3: 1020.

- Paasche E, Johansson S, Evensen DL. 1975. An effect of osmotic pressure on the valve morphology of the diatom *Skeletonema subsalsum* (A. Cleve) Bethge. *Phycologia* 14: 205–211.
- Pauly N, Knight MR, Thuleau P, Graziana A, Muto S, Ranjeva R, Mazars C. 2001. The nucleus together with the cytosol generates patterns of specific cellular calcium signatures in tobacco suspension culture cells. *Cell Calcium* 30: 413–421.
- Rosenwasser S, Graff Van Creveld S, Schatz D, Malitsky S, Tzfadia O, Aharoni A, Levin Y, Gabashvili A, Feldmesser E, Vardi A *et al.* 2014. Mapping the diatom redox-sensitive proteome provides insight into response to nitrogen stress in the marine environment. *Proceedings of the National Academy of Sciences, USA* 111: 2740–2745.
- Sarno D, Kooistra WHCF, Balzano S, Hargraves PE, Zingone A. 2007. Diversity in the genus *Skeletonema* (Bacillariophyceae): III. Phylogenetic position and morphological variability of *Skeletonema costatum* and *Skeletonema grevillei*, with the description of *Skeletonema ardens* sp. nov. *Journal of Phycology* 43: 156–170.
- Schneider CA, Rasband WS, Eliceiri KW. 2012. NIH Image to ImageJ: 25 years of image analysis. *Nature Methods* 9: 671–675.
- Schobert B. 1980. Proline catabolism, relaxation of osmotic strain and membrane permeability in the diatom *Phaeodactylum tricornutum*. *Physiologia Plantarum* 50: 37–42.
- Shabala SN, Lew RR. 2002. Turgor regulation in osmotically stressed *Arabidopsis* epidermal root cells. Direct support for the role of inorganic ion uptake as revealed by concurrent flux and cell turgor measurements. *Plant Physiology* 129: 290–299.
- Shen H, Li Z, Jiang Y, Pan X, Wu J, Cristofori-Armstrong B, Smith JJ, Chin YKY, Lei J, Zhou Q *et al.* 2018. Structural basis for the modulation of voltage-gated sodium channels by animal toxins. *Science* 362: eaau2596.
- Shen Y, Wu SY, Rancic V, Aggarwal A, Qian Y, Miyashita SI, Ballanyi K, Campbell RE, Dong M. 2019. Genetically encoded fluorescent indicators for imaging intracellular potassium ion concentration. *Communications Biology* 2. doi: 10.1038/s42003-018-0269-2.
- Stael S, Wurzing B, Mair A, Mehmer N, Vothknecht UC, Teige M. 2012. Plant organellar calcium signalling: an emerging field. *Journal of Experimental Botany* 63: 1525–1542.
- Supattapone S, Worley PF, Baraban JM, Snyder SH. 1988. Solubilization, purification, and characterization of an inositol trisphosphate receptor. *The Journal of Biological Chemistry* 263: 1530–1534.
- Takahashi K, Isobe M, Knight MR, Trewavas AJ, Muto S. 1997. Hypoosmotic shock induces increases in cytosolic Ca^{2+} in tobacco suspension-culture cells. *Plant Physiology* 113: 587–594.
- Taylor AR, Manison N, Fernandez C, Wood J, Brownlee C, Brownlee C. 1996. Spatial organization of calcium signaling involved in cell volume control in the fucus rhizoid. *The Plant Cell* 8: 2015–2031.
- Underwood G, Phillips J, Saunders K. 1998. Distribution of estuarine benthic diatom species along salinity and nutrient gradients. *European Journal of Phycology* 33: 173–183.
- Vardi A, Formiggini F, Casotti R, De Martino A, Ribalet F, Miralto A, Bowler C. 2006. A stress surveillance system based on calcium and nitric oxide in marine diatoms. *PLoS Biology* 4: e60.
- Verret F, Wheeler G, Taylor AR, Farnham G, Brownlee C. 2010. Calcium channels in photosynthetic eukaryotes: implications for evolution of calcium-based signalling. *New Phytologist* 187: 23–43.
- Yuan F, Yang H, Xue Y, Kong D, Ye R, Li C, Zhang J, Theprungsirikul L, Shrift T, Krichilsky B *et al.* 2014. OSCA1 mediates osmotic-stress-evoked Ca^{2+} increases vital for osmosensing in *Arabidopsis*. *Nature* 514: 367–371.
- Zhang M, Wang D, Kang Y, Wu JX, Yao F, Pan C, Yan Z, Song C, Chen L. 2018. Structure of the mechanosensitive OSCA channels. *Nature Structural and Molecular Biology* 25: 850–858.
- Zhao Y, Araki S, Wu J, Teramoto T, Chang Y-F, Nakano M, Abdelfattah AS, Fujiwara M, Ishihara T, Nagai T *et al.* 2011. An expanded palette of genetically encoded Ca^{2+} indicators. *Science* 333: 1888–1891.

Supporting Information

Additional Supporting Information may be found online in the Supporting Information section at the end of the article.

Fig. S1 Simultaneous imaging of R-GECO1 and GFP in fusiform *P. tricornutum* (PtR1-GFP) cells exposed to a hypo-osmotic shock treatment.

Fig. S2 Ca^{2+} responses to hypo-osmotic shock are dependent on the strength of the stimulus.

Fig. S3 Hypo-osmotic shock induces stimulus-strength specific spatial patterns of $[\text{Ca}^{2+}]_{\text{cyt}}$.

Fig. S4 Simultaneous imaging of R-GECO1 and GFP in oval *P. tricornutum* (PtR1-GFP) cells exposed to a hypo-osmotic shock treatment.

Fig. S5 The genetically encoded potassium biosensor GINKO1 is pH sensitive.

Methods S1 Generation of fluorescent *P. tricornutum* lines expressing R-GECO1, R-GECO1 with GFP and GINKO1.

Methods S2 Quantification of the Ca^{2+} dependency of organic osmolyte and K^{+} efflux in *P. tricornutum*.

Video S1 Ca^{2+} signalling responses of fusiform *P. tricornutum* cells being exposed to mild hypo-osmotic shocks.

Video S2 Ca^{2+} signalling responses of fusiform *P. tricornutum* cells being exposed to severe hypo-osmotic shocks.

Video S3 Ca^{2+} signalling responses of oval *P. tricornutum* cells to successive hypo-osmotic shocks.

Please note: Wiley Blackwell are not responsible for the content or functionality of any Supporting Information supplied by the authors. Any queries (other than missing material) should be directed to the *New Phytologist* Central Office.